Energy

Computational discovery of the top-performing zirconium based metal-organic framework for carbon dioxide capture

--Manuscript Draft--

Manuscript Number:	EGY-D-25-04472
Article Type:	VSI: Clean Energy Transition_Full length article
Section/Category:	Carbon Capture
Keywords:	High throughput screening; CO2 capture; Adsorption; Zirconium-based MOFs
Corresponding Author:	Sridhar Palla Indian Institute of Petroleum and Energy Visakhapatnam INDIA
First Author:	Iradat Hussain Mafat
Order of Authors:	Iradat Hussain Mafat
	Sridhar Palla
Abstract:	Zirconium-based MOFs (Zr-MOFs) are built by Zr-oxo clusters and conformational flexible linkers which could act as potential carbon dioxide (CO2) capture materials. Zr-MOFs have robust structures with excellent porosity, high specific surface area, and diverse functional groups feasible for CO2 gas separations. In this work, a screening study of the Zr-based MOFs for identifying top-performing MOFs for separating CO2 gas from the binary of CO2 and N2 is performed. Three types of adsorption conditions were investigated, such as pressure swing, vacuum swing, and temperature swing adsorptions. The top-performing MOFs for all three conditions were MOF-525, MOF-805, and Zr-DTDC. The structure-property relationships of MOFs were also studied to identify the best-suitable physical parameters of the MOF. The optimum range for the PSA condition was found to be 9.55 Å < largest cavity diameter < 16.26 Å, 4.22 Å < pore limiting diameter < 8.01 Å, 0.54 g/cm3 < density < 0.91 g/cm3, 0.59 < void fraction < 0.74. Density functional theory (DFT) calculations were conducted on MOF-805 to understand the adsorption of CO2 and N2 gas molecules.The Zirconium metal sites and naphthalene di carboxylate linkers are discovered as the adsorption active sites for CO2 and N2 on the MOF-805.

Computational discovery of the top-performing zirconium based metal-organic framework for carbon dioxide capture

Iradat Hussain Mafat [a], Sridhar Palla [a*]

[a] Department of Chemical Engineering, Indian Institute of Petroleum and Energy, Visakhapatnam-530003, India

[*]Corresponding Author: Sridhar Palla (sridharpalla.che@iipe.ac.in)

Abstract

Zirconium-based MOFs (Zr-MOFs) are built by Zr-oxo clusters and conformational flexible linkers which could act as potential carbon dioxide (CO_2) capture materials. Zr-MOFs have robust structures with excellent porosity, high specific surface area, and diverse functional groups feasible for CO_2 gas separations. In this work, a screening study of the Zr-based MOFs for identifying top-performing MOFs for separating CO_2 gas from the binary of CO_2 and N_2 is performed. Three types of adsorption conditions were investigated, such as pressure swing, vacuum swing, and temperature swing adsorptions. The adsorbent performance score and regenerability were the metrics used to rank the materials in this screening study. The top-performing MOFs for all three conditions were MOF-525, MOF-805, and Zr-DTDC. The structure-property relationships of MOFs were also studied to identify the best-suitable physical parameters of the MOF. The optimum range for the PSA condition was found to be 9.55 Å < largest cavity diameter < 16.26 Å, 4.22 Å < pore limiting diameter < 8.01 Å, 0.54 g/cm^3 < density < 0.91 g/cm^3, 0.59 < void fraction < 0.74. Density functional theory (DFT) calculations were conducted on MOF-805 to understand the adsorption of CO_2 and N_2 gas molecules. The adsorption binding energies, enthalpy, and vibrational frequencies were estimated by the DFT study. The Zirconium metal sites and naphthalene di carboxylate linkers are discovered as the adsorption active sites for CO_2 and N_2 on the MOF-805. The adsorption energy of CO_2 molecules populated in the 9 active sites of the MOF-805 framework according

to the preferential sites is -24.34 kJ/mol which is close to the CO_2 heat of adsorption estimated by Grand Canonical Monte Carlo calculation i.e. -24.92 kJ/mol.

Keywords: *High throughput screening, CO_2 capture, Adsorption, Zirconium-based MOFs*

1. Introduction

Rapid growth in industrialization and human civilization consumes significant fossil fuels which enhanced the carbon emissions worldwide [1]. Coal-fired power stations, Natural gas power plants, cement industries, and crude oil refineries are the major CO_2 contributors. Carbon capture and storage (CCS) is a promising solution to mitigate CO_2 emissions by promoting carbon capture and sequestration techniques. Among the several post-combustion capture strategies in the CCS, the adsorption-separation method is one of the most efficient and has been adopted by industries [2]. Adsorption offers a low regeneration heat, high CO_2 selectivity, fast kinetics, and reusability for a wide range of working conditions. The affinity of the CO_2 towards the adsorbent is the driving force that separates CO_2 present in the flue gas. Selecting the adsorbent with high CO_2 storage capacity, CO_2 selectivity, and fast kinetics between CO_2/N_2 is essential. Recent developments in adsorption and separation technologies have led to the swift evaluation and diversification of many sorbent material types. These sorbent materials are widely used in a variety of sectors, including metallurgy, food production, pharmaceuticals, petrochemicals, and environmental protection. Adsorbents such as metal oxides, zeolites, activated carbon, and metal-organic frameworks were thoroughly investigated for the separation of CO_2 gas [3,4].

MOFs are a versatile class of nanoporous materials that received significant attention from the academic and industrial communities for the past two decades [5–7]. These are high-porous materials created by metal ion clusters combined with organic linkers. Researchers in this community explored this unique combination of the metal cluster and organic linker and produced hundreds of thousands of MOFs. These structures provide uncharted areas of MOF

structure and chemistry, which helps to progress material science research. Researchers can concentrate on the most promising options for the different storage and separation applications by maintaining a range of designs. In the process of the multiple metal cluster and linker combination, datasets, such as Wilmer's hypothetical MOFs [8], computational ready MOFs [9], Boyd's hypothetical MOFs [10], and topological-based crystal constructors (ToBaCCo) [11], were reported. However, several MOFs are reported in these databases, the majority are unexplored for carbon capture due to the complexity involved in the experimental and theoretical investigation of the large datasets. High throughput computational screening is developed as a viable option to overcome this challenge [12]. The high-throughput screening approach utilizes computational tools such as molecular simulations and density functional theory (DFT) to predict MOFs' physical, chemical, and adsorbent characteristics. The estimated properties are used as performance metrics to rank the adsorbent material for carbon capture.

Zirconium-based MOFs have been utilized to identify promising MOFs in various applications such as mercury separation, methane storage, and many more. This MOF database addresses certain structural instabilities [13]. For the MOFs in practical applications which are ascribed to the reversible nature of coordination bonds between metal ions and organic ligands [14]. Many steps were taken to improve the inherent stability of MOFs. One of the remarkable steps is the discovery of the archetypal zirconium (IV) based "UiO" series of MOFs in 2008 by Cavka et al. [15]. This series consists of the Zr_6O_8 inner cores that are strongly bound to 12 dicarboxylate-type ligands. Further, the discovery of novel Zr-based MOFs has enhanced the field of material science yielding a variety of materials with multiple topologies [16,17]. Apart from that, there are numerous other nodes such as Zr_6, Zr_8 [18], and dimeric Zr_{12} clusters reported in the literature [19].

Zr-MOFs have excellent structural properties such as robust skeleton, ultra-high surface area, improved pore structure, and are well-structured, which allows them to provide versatility

in chemistry applications. Due to their high charge density of Zr_4 and bond polarization, they have strong bonding interactions with O atoms in the ligands. Previous studies showed that the Zr-MOFs have high water resistance [20,21] and organic solvents [22,23] which would be best fit for carbon capture under humid conditions. One of the Zr-based MOFs (NU-1103) is found to have a very high specific surface area of around 6550 m^2/g [24]. These materials' high specific surface area and pore size are the two important structural features that make them more suitable for gas storage and separation applications. Apart from that, pore volume and diameter also play a critical role in capturing gases. The pore size of Zr-MOFs can be elaborately tailored by controlling the length of organic ligands [15]. Control over functionality and pore tunability offers Zr-MOFs a suitable design for a wide range of applications. The structure of these MOFs can be adjusted according to the specific target adsorbates for improving the adsorption force of attractions between MOFs and guest molecules. In the case of flue gas separation, the selectivity of CO_2 gas can be improved by the addition of specific adsorption sites such as amino groups [25,26], carboxyl groups [27], hydroxy groups [28], etc. These functional groups can significantly enhance the interactions between materials and CO_2 guest molecules with the help of hydrogen bonding, π–π stacking, coordination interaction, and electrostatic interaction [23]. To improve structural properties, defect engineering can also enhance the Zr-MOFs functionality, aiding in better adsorption and separation [29].

The screening of Zr-MOFs for the identification of top-performing Zr-MOFs can reduce the experimental efforts of the researchers. Very few screening studies have been performed previously to identify top-performing Zr-based MOF for the various adsorption applications, as explained in **Table 1**. The Zr-MOF database was constructed by Gomez-Gualdron et al. (2014), who performed the initial screening study for the storage of CH_4 in natural gas. A total of 204 MOFs featuring $(Zr_6O_4)(OH_4)(CO_2)_n$ inorganic building blocks were used in this study. From the performed screening study, it was found that the CH_4 deliverable

capacity of NU-800 between 65 bar and 5.8 bar was around 0.215 g/g which was found to be the highest among all Zr-based MOFs [30]. In 2019, Zhou et al. performed a screening study for the separation of H_2S from the binary mixture of H_2S and CH_4. They utilized a total of 182 experimentally synthesized Zr-MOF structures with more than 10-coordinated Zr_6O_8 nodes. The LIFM-29 MOF was identified to be the best Zr-MOF for the separation of H_2S which exhibited a high H_2S/CH_4 selectivity of 269 and high working capacity (ΔN) at 1 bar and 10 bar pressure [31]. Oktavian et al. (2022) performed a screening analysis with the help of 102 Zr-oxide MOFs for the capturing of CO_2 from the flue gas mixture. Periodic density functional theory calculations were also performed which compared 25 different combinations of basis sets and functionals to calculate framework particle atomic charges [32]. Qi et al. (2023) utilized 181 Zr-based MOFs for screening the best material for the separation of mercury from the industrial flue gas. The study concluded with the two best-performing MOFs for the capturing of mercury which have high Grand Canonical Monte Carlo (GCMC) selectivity of 4.64 and 4.55, respectively by UiO-66-$(SO_3H)_2$ and MOF-801 [33].

Table 1. The previous screening was performed for the identification of top Zr-MOF.

Dataset quantity	Criterion parameters	Target adsorbates	Top-performing MOFs	Reference
204 $(Zr_6O_4)(OH_4)(CO_2)_n$ inorganic blocks	CH_4 deliverable capacity	Pure CH_4	Highest CH_4 deliverable capacity by NU-800 of 0.215 g/g	[30]
182 Zr_6O_8 nodes 10-coordinated structures	Selectivity of H_2S/CH_4, ΔN_{H2S}, and APS	H_2S from the binary mixture of H_2S and CH_4	Highest selectivity of 269 by LIFM-29	[31]
102 Zr-oxide node structures	CO_2 uptake	CO_2 from the binary mixture of CO_2 and N_2	MOF-812	[32]
181 Zr-MOFs	Hg uptake, Hg/SO_2 selectivity, and Henry's selectivity	Hg from the binary mixture of Hg and SO_2	Highest Hg^o selectivity of 4.64 and 4.55 by UiO-66-$(SO_3H)_2$ and MOF-801 respectively	[33]

The literature study lacks the screening of Zr-based MOFs for capturing low-concentration CO_2 gas from the industrial flue gas mixture based on performance metrics such as adsorbent performance score and regenerability. This study uses a stepwise screening methodology to identify top-performing Zr-based MOFs (CO_2:N_2 = 20:80) with the help of the high throughput screening technique. The adsorption performance of Zr-based MOFs is simulated, and the structure-activity relationships for the different geometrical properties are also analyzed, which can be useful for designing NEW Zr-MOFs, with enhanced properties. For this study, GCMC simulations under three different adsorption conditions, i.e. pressure swing adsorption (PSA), vacuum swing adsorption (VSA), and temperature swing adsorption (TSA) are performed. Comprehensive screening criteria are employed to isolate top-performing MOFs based on the factors that affect industrial efficiencies such as CO_2 uptakes, ΔN_{CO2}, CO_2/N_2 selectivity, adsorbent performance score, and regenerability. Based on the performance metrics, the top 10 performing Zr-based MOFs are identified, which can be applied in various large-scale applications to capture CO_2. This screening study is useful for the scientific community working in MOFs to identify top-performing MOFs for various gas separation applications by rapidly evaluating multiple adsorbent structures. Research communities can benefit from the top-performing MOFs found in this work since they can concentrate on the high-potential Zr-based MOFs found using a computational method rather than synthesizing random MOFs. The identified MOFs are useful even for other adsorption applications such as coal gasification or pre-combustion capture.

2. Computational model and details

2.1 MOF database, characterization, and pre-screening

A total of 182 crystallographic information files (CIFs) were generated by the computational screening performed by Gomez-Gualdron et al. (2014) [30]. They utilized a reverse topological approach [34], in which, the four topological nets fcu, ftw, scu, and csq

were used as the templates for the development of Zr-based MOFs with the help of multiple building blocks such as linear ditopic, planar tetratopic, central, and peripheral building blocks. Different types of geometric features are considered very crucial for the separation process of CO_2 and N_2 molecules. In this study, physically intuitive and computationally feasible features such as largest cavity diameter (LCD), pore limiting diameter (PLD), accessible surface area (ASA), density, and void fraction (VF) are incorporated. The VF is calculated with the RASPA code [35]. The remaining structural parameters, such as LCD, PLD, ASA, and density, are computed with the Zeo++ program [36].

2.2 Molecular simulation

The molecular simulation studies are performed with the Grand Canonical Monte Carlo (GCMC) simulation to replicate the adsorption behavior of the CO_2 and N_2 gas in the 182 Zr-based MOFs. The gas loading capacities of each component in the binary mixture are estimated by adjusting the bulk pressure, temperature, and gas mixture compositions in the GCMC simulations. The operating parameters required for the different adsorption studies performed in this study are explained in **Figure 1**. Three different adsorption conditions are performed in this study, consisting of pressure swing adsorption (PSA), vacuum swing adsorption (VSA), and temperature swing adsorption (TSA). In the PSA simulations, the bulk pressure values are adjusted to 6 bar for the adsorption, and 1 bar for the desorption process with a simulation temperature of 298 K for both, adsorption and desorption conditions [37]. Similarly, for the VSA conditions, the bulk pressure is adjusted to 1.5 bar (adsorption) and 0.05 bar (desorption) at the temperature value of 298 K. However, for the TSA condition, the pressure value is kept constant at 1.11 bar and the temperature varies from 308 K (adsorption) to 383 K (desorption)[38]. The mole fraction of the CO_2 and N_2 gas mixture is set to 0.2 and 0.8 respectively, corresponding to the practical applications in the flue gas industries for all three cases. In this study, short-range van der Waals interactions are considered which are calculated

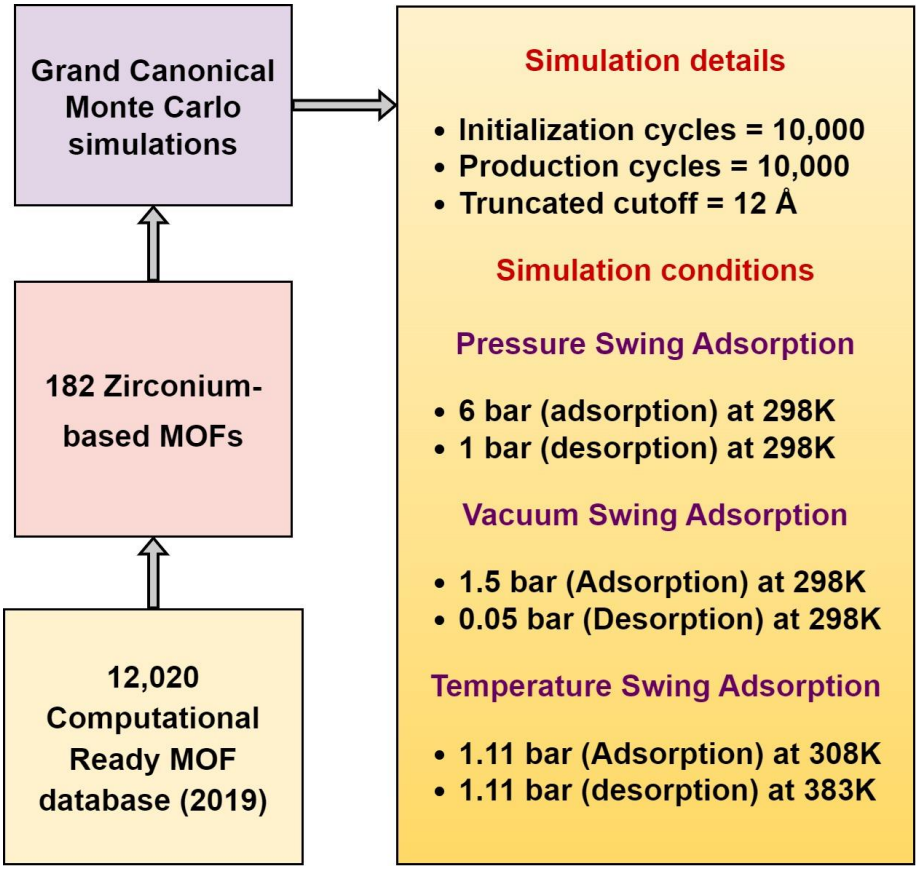

Figure 1. Simulation procedure for the PSA, VSA, and TSA conditions.

based on the Lennard-Jones (LJ) potential and are truncated at the cutoff distance of 12 Å. The partial atomic charges of MOF atoms were assigned by the charge equilibration method [8]. The LJ parameters for the CO_2 and N_2 molecules are listed in **Table 2**. The CO_2 molecule is represented by the EPM2 model which was proposed by Harris and Yung (1995) [39]. It is a rigid and linear model with three charged sites entered on each atom and a C-O distance of 1.16 Å. Similarly, the N_2 molecule is modeled as a diatomic molecule with a fixed bond length of 1.1 Å. In this model, the point charges are centered on each LJ site, and electric neutrality is maintained by placing a point charge at the center of the mass of the N_2 molecule. The LJ parameters of the N_2 molecule were taken from the TraPPE forcefield [40]. The LJ parameters are based on the Universal Force Field (UFF) and are adapted for the MOF structure atoms [41].

The RASPA simulation tool [35] is used to perform simulation studies of the adsorption of CO_2 and N_2 in the Zr-based MOFs. A total of 20,000 cycles are carried out in each GCMC simulation. The initial 10,000 cycles are performed for the equilibration while the later 10,000 are for the calculation of the average thermodynamic properties [42]. It has also been found that the increasing number of cycles has significantly no effect on the result, however, it consumes more computational resources. For each GCMC simulation cycle, four types of trail moves with equal probabilities were considered for the adsorbate gas molecules. They include random translation, rotation, reinsertion, and swapping. A validation study for the parameter settings for the GCMC simulation is also performed, and the single component adsorption isotherm for the pure CO_2 and N_2 for MOF UiO-66 is also conducted based on the parameter settings.

Table 2. LJ Potential Parameters for Adsorbate-Adsorbate Interactions.

	atom-atom σ (Å)	atom-atom ε/k_B (K)	Reference
$\mathbf{O_{CO2}}$	3.033	80.04	[39]
$\mathbf{C_{CO2}}$	2.767	27.69	
$\mathbf{N_{N2}}$	3.31	36	[40]

2.3 Density Functional Theory Calculation

Vienna Ab intio Simulation Package (VASP) is used to perform the Density Functional Theory (DFT) calculations [43–46]. The energy cutoff of 600 EV is used for the plane wave basis set during simulations. Projector augmented wave (PAW) [47] is applied for core and valence electron interaction. Perdew-Burke-Ernzehof (PBE) [48] exchange-correlation functional with Grimme's DFT-D3 dispersion interaction with Becke-Johnson damping corrections [49] is used in DFT calculations, which integrates the DFT-D3 functional. This study investigates MOF-805 (top-performing MOF for the VSA condition) by DFT calculations to validate with molecular simulation energies and analyze the active sites. MOF-805 CIF is obtained from the Cambridge Crystallographic Data Centre (CCDC) [50]. The

binding energies of the gas molecules CO_2 and N_2 are calculated for different sites by following **Equation 1**

$$\Delta E_{ads} = E_{total} - \left(E_{MOF805} + E_{CO_2 or N_2}\right) \quad \textbf{(1)}$$

E_{total} represents the total energy of the MOF-805 and guest molecule, either CO_2 or N_2, in the system. The E_{MOF805} and E_{CO_2/N_2} represents the energies of the MOF-805 and CO_2 or N_2 molecules respectively. The energies obtained in this study are considered after geometry optimization. The adsorption energy was estimated as the sum of the binding energies, zero-point energy (ZPE), and temperature correction as shown in **Equation 2** below.

$$\Delta H_{ads} = \Delta E_{total} + \Delta ZPE + \int_0^T C_P dT \quad \textbf{(2)}$$

The zero-point energy (ZPE) correction was calculated as given in the **Equation 3**

$$\Delta ZPE = \sum_{i=1}^{n} \frac{h v_i}{2} \quad \textbf{(3)}$$

In **Equation 3**, v_i represents the vibrational frequency, and n represents the number of vibrational frequencies incorporated for the adsorbed species. The gas molecules CO_2 and N_2 vibrational frequencies are estimated for free molecules and adsorbed molecules to estimate the difference. The third term in **Equation 3** is the temperature correction term, which contains the heat capacity at a constant temperature.

2.4 Performance Metrics Evaluation

The MOF adsorbent materials' separation capability is evaluated with metrics such as working capacity (ΔN_{CO2}), adsorption selectivity of CO_2/N_2 mixture, adsorbent performance score, and regenerability of MOFs. The output from the GCMC simulations consists of uptakes at adsorption and desorption pressure and temperature range. The simulated uptakes are then used to calculate the ΔN_{CO2} and ΔN_{N2}. The ΔN measures the difference between the uptake amount of CO_2 and N_2 at different conditions. The high value of ΔN represents that more

quantity of targeted guest molecules can be acquired through the MOFs. The selectivity of CO_2 from the binary mixture is also a crucial parameter which refers to the ability of MOF to adsorb CO_2 over N_2 gas preferentially. Similarly, the adsorbent performance score is also a performance metric that evaluates the efficiency of the MOF material. This parameter is mostly utilized for material screening applications such as gas separations, which play a remarkable role as the trade-off between the ΔN and selectivity of the material [51]. The formula for all of the performance metrics is shown in **Table 3**.

Table 3. Performance metrics utilized in this study.

Performance metrics	Formula
Working capacity	$\Delta N_i = N_{ads,i} - N_{des,i}$
Adsorption selectivity	$S_{ads,CO2/N2} = \frac{(N_{CO2} * y_{N2})}{(N_{N2} * y_{CO2})}$
Adsorbent performance score	$APS = S_{ads,CO2/N2} * \Delta N_{CO2}$
Regenerability (%)	$R\% = \frac{\Delta N_{CO2}}{N_{ads,CO2}} * 100\%$

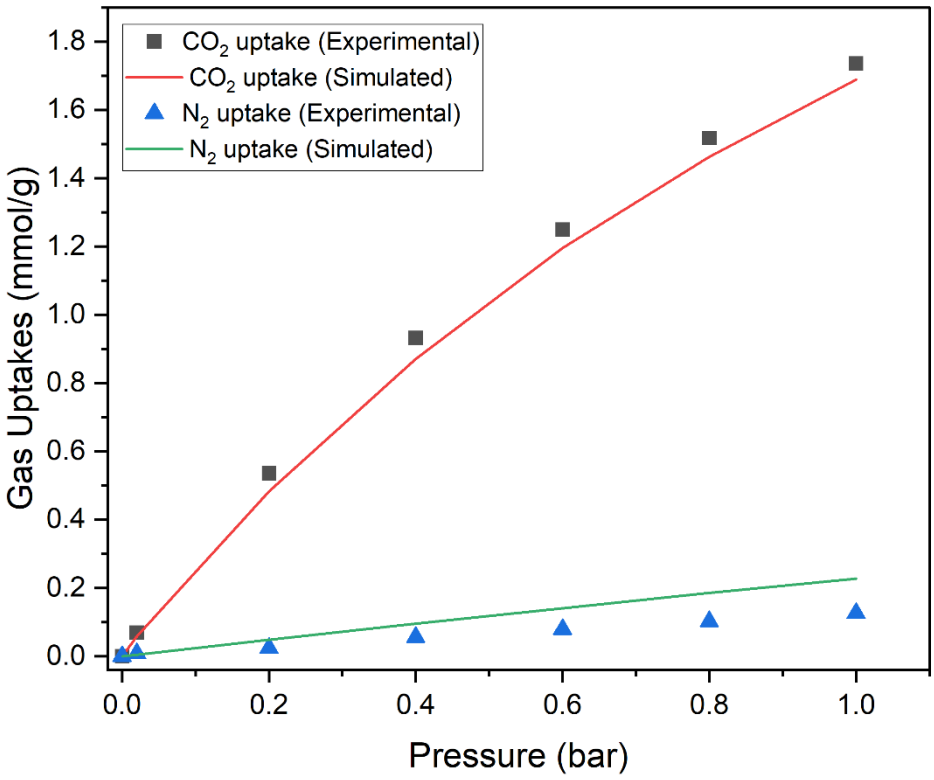

3. Results and Discussion

3.1 Comparison of experimental and simulation results

The accuracy of GCMC simulations is validated by comparing the single-component gas adsorption of CO_2 and N_2 on MOFs with the experimental dataset performed by Cmarik et al. (2012) [52]. The experimental data is performed for the UiO-66 MOF which was simulated on the pressure values from 0 bar to 1 bar pressure at 298K. **Figure 2** compares experimental uptakes by Cmarik et al. (2012) and the GCMC simulated uptake used in this study. From the generated plot, it can be found that there is a good agreement between the experimental and simulated measurements for both CO_2 and N_2 uptakes. It can be observed that the CO_2 model proposed by Harris and Yung (1995) and the N_2 model by the TraPPE are found to show better agreement with the experimental values. The validated GCMC simulation parameters are utilized for the further calculations.

3.2 Top-performing MOFs

Figure 2. Forcefield verification of UiO-66 with the help of chosen LJ parameters.

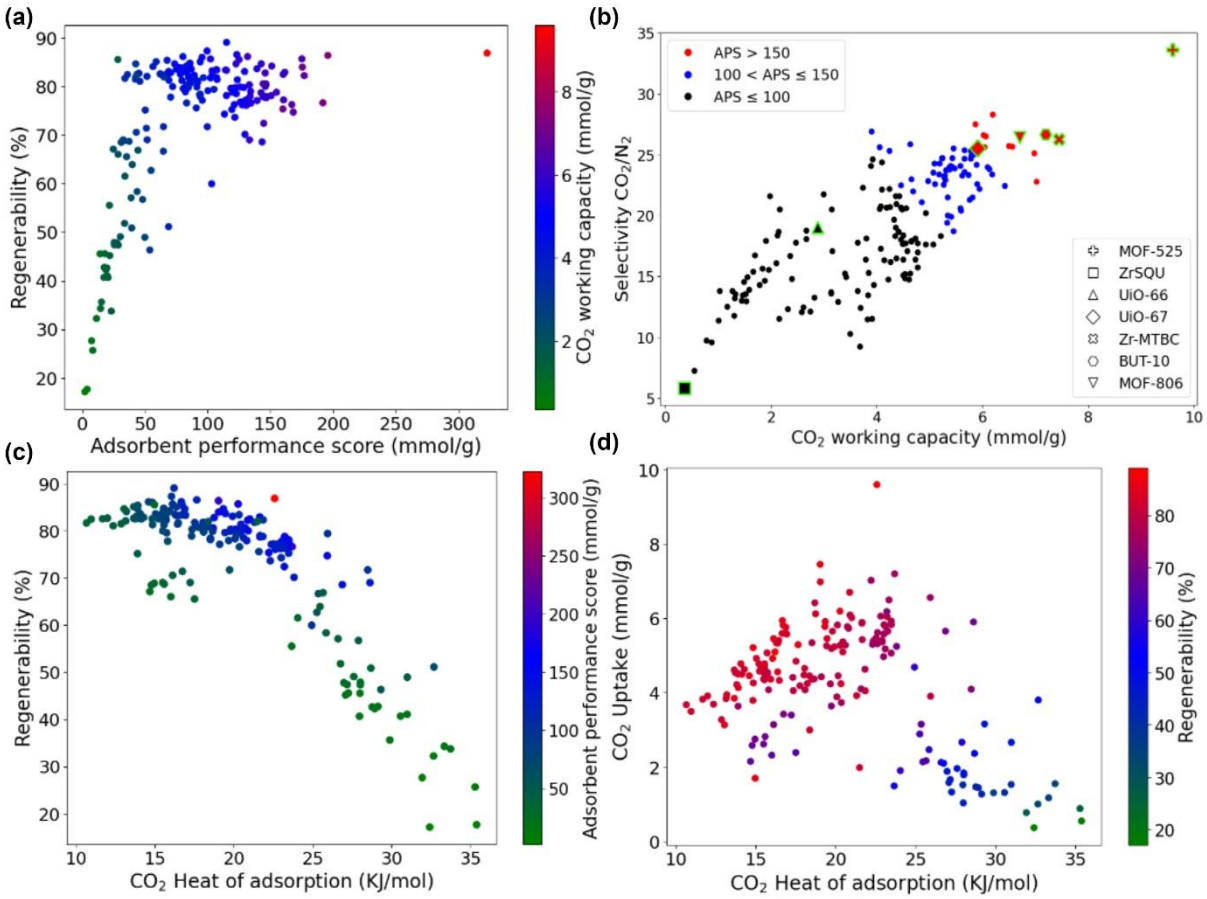

Figure 3. Distribution of Zr-based MOFs in performance metrics space for PSA (a) Regenerability v/s APS, (b) CO_2/N_2 Selectivity v/s ΔN_{CO2}, (c) Regenerability v/s CO_2 heat of adsorption, and (d) CO_2 uptake (6 bar) v/s CO_2 heat of adsorption.

The GCMC simulations for the Zr-based MOFs are performed for the three adsorption conditions, i.e. PSA, VSA, and TSA. In the PSA condition, the adsorption pressure is taken as 6 bar pressure, while the desorption pressure is chosen as 1 bar at room temperature. **Figures 3 (a)**, **(b)**, **(c)**, and **(d)** show different plots that are developed with estimated performance metrics from the output file generated from the GCMC simulations. These plots show the distribution of 182 MOF separation performance metrics for the PSA conditions. From **Figure 3 (b)**, it can be found that there exist many MOFs, such as NU-1103 which provided a high ΔN_{CO2} value of 3.9 mmol/g; however, the CO_2/N_2 selectivity for this MOF resulted in around 11.5. Therefore, it can be observed that despite high ΔN, it might not be an advantageous option in practice as the corresponding selectivity is relatively low. The high interaction of CO_2 with the MOFs might also result in stronger interactions with the N_2 which could lead to the reduced

CO_2/N_2 selectivity [53]. A trade-off between the ΔN and selectivity can be resolved with the adsorbent performance score. Therefore, in **Figure 3 (b)**, the contour plot is divided into three color ranges, i.e. black, blue, and red. The black indicates the MOFs with APS value less than 100 mmol/g, blue indicates APS values between 100 mmol/g and 150 mmol/g, and red indicates the APS value greater than 150 mmol/g. From the 3rd segment, which is the red colors, it can be seen that the highest APS score is obtained by MOF-525, which provided relatively high ΔN and CO_2/N_2 selectivity compared to other MOFs. The APS score for MOF-525 is found to be around 322.76 mmol/g. The ΔN_{CO2} and selectivity are 9.59 and 33.62, respectively, which is relatively high compared to other MOFs. The highest CO_2 uptake value of 11.04 mmol/g and low N_2 uptake value of 1.31 mmol/g at the adsorption pressure value is provided by the MOF-525. However, in terms of large-scale applications, the regenerability of the MOFs becomes very critical as it specifies the significant loss in the performance of MOFs after the number of cycles. **Figure 3 (a)** visualizes the Zr-MOF in the perspective of regenerability and APS with a heatmap of ΔN_{CO2}. It can be observed that the MOF-525 provided 3rd highest regenerability compared to the remaining MOFs with a value of 86.86 %. The highest regenerability is provided by the MOF named ZrOMTP (89.06 %). However, the ΔN_{CO2} for this MOF is 5.09 mmol/g, which is comparatively lower than MOF-525. The list of top 10 MOFs with the highest APS are listed in **Table 4**. From a similar plot, it can also be observed that the lower values of HOA adsorption resulted in lower CO_2 uptakes. The low HOA indicates that the CO_2 molecules are weakly bound with the MOF surface which results in easy detachment from the surface. **Figure 3 (d)** visualizes the relationship between the CO_2 uptake and the CO_2 heat of adsorption with the variation in the regenerability. The heat of adsorption and MOFs' regenerability are highly interconnected, as high HOA indicates a stronger interaction between CO_2 and MOF. It can lead to the complication of regenerability by increasing the heat of desorption during the regeneration process [54]. From **Figure 3 (d)**, it

can be implied that the increase in the HOA value results in the reduction of the regenerability of MOF. The lowest regenerability value of 17.14% is provided by an MOF named ZrSQU which provided a comparatively high HOA value of 32.41 kJ/mol. Therefore, an optimum range exists for the HOA value to obtain the highest CO_2 uptake at adsorption conditions and regenerability for the Zr-based MOFs [55]. In the case of PSA conditions, the Zr-MOFs with HOA values existing in the range of 20 kJ/mol and 25 kJ/mol provided the best ΔN_{CO2}. The highest CO_2 was obtained by MOF-525, which provided an HOA value of 22.58 kJ/mol. **Figure 3 (c)** also indicates the relationship of HOA with regenerability, but APS is kept as the heatmap variable. This plot also indicated that the APS value for the various MOFs is optimum when the HOA values range from 20 to 25 kJ/mol.

Table 4 contains the list of the top 10 performing Zr-based MOFs for the PSA, along with their performance metrics and geometrical characteristics. A lot of common properties are identified in this list such as the presence of certain functional groups, polarization, electrostatic, and quadrupole interactions. MOFs such as UiO-67-Cl, UiO-67-BN, and Zn-DPDBP-UiO possess functional groups such as chlorine and boron nitride which increase polarity and Lewis acidic sites of the overall MOF structures. This enhancement aids in the stronger interaction between the dipoles of the polar groups and quadrupoles of CO_2 molecules which results in better adsorption [56]. Functional groups that impart Lewis acidity to the MOFs can interact more effectively with the CO_2, which is basic. The electronegative nature of chlorine increases the charge symmetry while the BN functional group can create Lewis acidic sites within the frameworks [57]. Similarly, other MOFs such as MOF-525 and MOF-805 possess extremely high surface area. The large pore volumes and combination of mesopores and micropores allow for high CO_2 capacity and rapid gas diffusion as it allows the accommodation of more gas molecules without steric hindrance. The mesopores serve as the larger channels that connect the micropores to improve the transportation of CO_2 molecules.

This ideal combination of pore sizes can also improve the selectivity for CO_2 over the N_2 gas molecules as the distinct size and connectivity of pores can enable preferential adsorption behavior. Apart from the structural properties, both of the MOF possess carboxylate functional groups on their organic linkers (tetrakis (4-carboxyphenyl) porphyrin (TCPP) for MOF 525 and 1,3,5-benzenetricarboxylate (BTC) for the MOF-806). The TCPP contains 4 carboxylate groups, with one in its 4 phenyl rings, while BTC contains 3 carboxylates around the benzene rings. This carboxylate contributes to the stability of the MOF structure which also maintains the porosity during CO_2 capturing [58]. The organic linkers in MOFs such as Zr-MTBC (4 carboxylate groups), Zr-CCA (2 carboxylate groups in cis configuration), and Zr-BTDC (2 carboxylate groups attached thiophene ring) are also performing well for the capturing of CO_2 molecules. Carboxylate ligands contribute towards the structural stability of the MOFs resulting in a robust framework that endures the stress during CO_2 adsorption. The conformational flexibility of the methane-tetrakis (p-biphenyl carboxylate) (MTBC) linker allows the framework to adapt under various conditions, improving the CO_2 adsorption capacity. This carbonyl oxygen in this linker can interact with Lewis acidic sites found in specific metal centers within the MOF, which leads to the formation of metal-coordinated complexes that enhance the CO_2 interaction [59]. The MOF Zr-CCA (cis-cis-muconic acid)

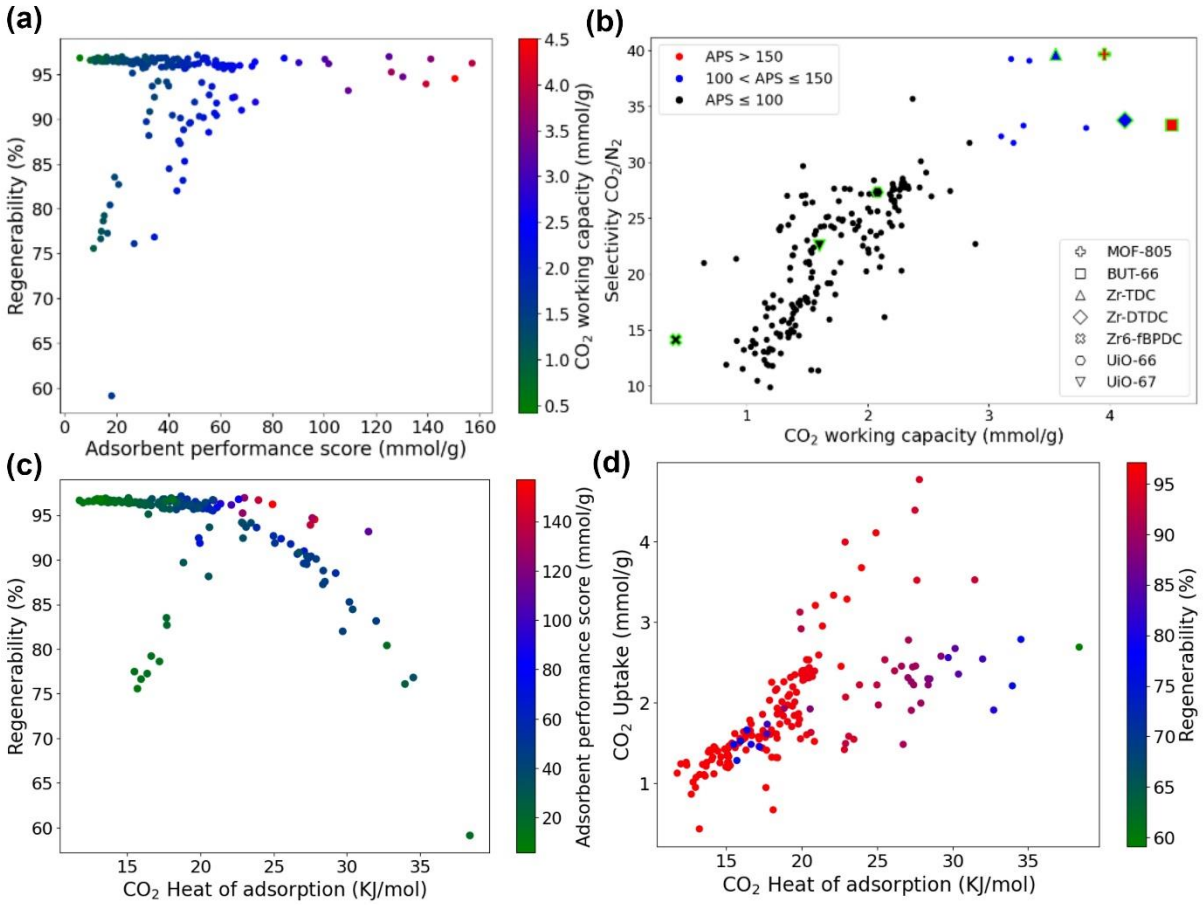

Figure 4. Distribution of Zr-based MOFs in performance metrics space for VSA (a) Regenerability v/s APS, (b) CO_2/N_2 Selectivity v/s ΔN_{CO2}, (c) Regenerability v/s CO_2 heat of adsorption, and (d) CO_2 uptake (6 bar) v/s CO_2 heat of adsorption.

exhibits extreme thermal stability which enables it to withstand high temperatures without distortion in its structural properties.

Similarly, **Figure 4** shows the distribution of Zr-based MOFs in the performance metric space for the VSA simulation. The VSA simulation is performed for the adsorption value of 1.5 bar and desorption value of 0.05 bar pressure at room temperature. From the **(a)** plot of **Figure 4**, it can be seen that a high regenerability value of more than 90% is observed from nearly 158 MOFs. The least regenerability value of 59% is provided by a MOF named UiO-66-$(SO_3H)_2$ which becomes the most unsuitable MOF for the VSA application for capturing CO_2. The highest regenerability is provided by the MOF Zr-CCA which is also found to be the top-performing MOF for the PSA condition. It gave a very high regenerability value of 97.1 %, indicating the increased number of cycles for the large-scale application. However, Zr-CCA

MOF provided a low APS value of 51.1 mmol/g. **Figure 4 (b)** shows that only two MOFs are giving the APS score of more than 150 mmol/g, i.e. MOF-805 (157 mmol/g) and BUT-66 (150 mmol/g). Most of the MOFs tend to provide APS values less than 100 mmol/g. MOF-805 provided the highest CO_2/N_2 selectivity of 39.72 with the CO_2 uptake at an adsorption value of 3.95 mmol/g which is found to be the highest among all Zr-based MOFs. The MOF BUT-66 gave the selectivity value of 33.35 with the highest CO_2 uptake value of 4.5 mmol/g. Both of the MOFs provided comparatively better regenerability values of 96.21 % and 94.51 % for the MOF-805 and BUT-66 respectively. From the **(c)** plot of **Figure 4**, which shows the relationship between the regenerability of MOF and heat of adsorption, it can be found that the highest regenerability of MOFs for the VSA is found to be over 97% by Zr-CCA, however, the APS values are found to be lower in that region. The MOFs with the highest range of APS values are found with the heat of adsorption value in the range of 23 kJ/mol to 28 kJ/mol, the MOF-805 provided low heat of adsorption value of 24.92 kJ/mol. The other MOFs such as NU-801, NU-800, and MOF-525, gave very high regenerability of over 96% with the heat of adsorption values less than 18 kJ/mol, however, these MOFs turned out to be low performing in terms of APS values which lies lower than 50 mmol/g. The highest heat of adsorption is achieved by the MOF with the lower regenerability as the increase in the heat of adsorption results in strong interactions between CO_2 and MOF structure which increases the difficulty in the regeneration. **Figure 4 (d)** shows the relationship between the ΔN_{CO2} and the CO_2 heat of adsorption. It can be found that the MOFs with the heat of adsorption in the range of 23 kJ/mol to 28 kJ/mol are found to be the adsorbents with the highest uptakes and high regenerabilities. However, the least CO_2 uptake (0.41 mmol/g) is given by the MOF with the HOA value of 13.21 kJ/mol which indicates that the lower HOA value results in the reduction of interaction between MOFs and CO_2 molecules which reduces the CO_2 uptake values.

Table 5 lists the top-performing Zr-based MOFs for the VSA conditions based on the APS values. From the table, it can be found that the MOF named MOF-805 gave the highest APS value of 157.05 mmol/g with a CO_2/N_2 selectivity of 39.72. One of the common attributes among all top 10 MOFs except the TBP-MOF(Cu) is found that all MOF contains the carboxyl group on the organic linkers which aids in the enhancement of pi-pi interactions with polar gases, especially CO_2 which results in better adsorption. The top-performing MOFs for the PSA conditions also indicated the presence of carboxyl groups can improve the target gas uptakes. The presence of thiophene rings or modified thiophene rings with the methyl groups in the MOFs such as Zr-TDC (Zr-thiophene-2,5-dicarboxylate) and Zr-DTDC (Zr-2,5-dimethlthiophene-2,5-dicarboxylate) are also found which provides the electron-rich sites due to the presence of sulfur in their structures. The sulfur atom which has a lone pair of electrons can effectively interact with the electrophilic carbon atom of CO_2 which increases the adsorption capacities [60]. Similarly, the methyl groups are electron-donating substituents which when attached to the thiophene rings increase the overall density of the MOF structure [61]. The rich thiophene interacts with the electron-deficient CO_2 molecule which enhances the ΔN_{CO2} and CO_2/N_2 selectivity. One of them is named MOF-812 which consists of biphenyl-4,4'-dicarboxylate (BPDC) and 2-amino terephthalate (NH_2-BDC) linkers. The basic nature of amines can result in the formation of carbamate species which can significantly increase the binding affinity of CO_2 and MOFs [62]. The presence of NH_2-BDC can also be functionalized with other groups such as polyamines which can result in the enhancement of CO_2 adsorption

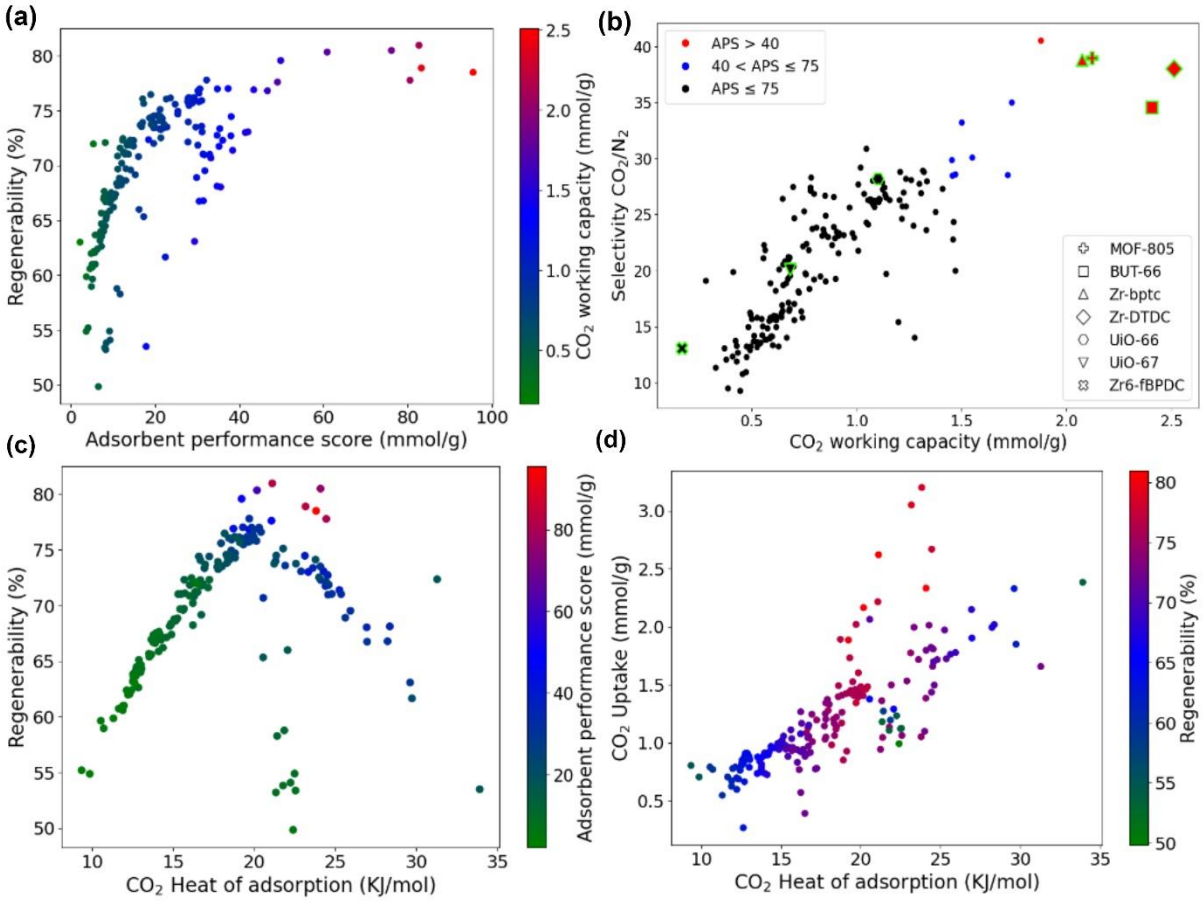

Figure 5. Distribution of Zr-based MOFs in performance metrics space for TSA (a) Regenerability v/s APS, (b) CO_2/N_2 Selectivity v/s ΔN_{CO2}, (c) Regenerability v/s CO_2 heat of adsorption, and (d) CO_2 uptake (6 bar) v/s CO_2 heat of adsorption.

capability which improves the MOF performance without any functionalization or with easy linking groups.

Figure 5 shows the variation of different features for the TSA conditions. The TSA simulation is performed at a temperature value of 383K for the adsorption process and 308K for the desorption at the pressure value of 1.11 bar. Compared to the PSA and VSA conditions, the TSA simulations provided lower values of APS. The **(a)** plot of **Figure 5** also indicates the regenerability value tends to be on the lower side compared to other conditions. In the TSA condition, the heat is transferred efficiently and uniformly to the adsorbent to achieve effective desorption. However, slow or inefficient heat transfer can lead to incomplete desorption which results in residual adsorbed species that impact subsequent adsorption cycles [63]. The high regenerability is obtained by MOF-805 with a value of 80.96%. The GCMC-generated

molecular structure of the MOF-805 with the captured CO_2 and N_2 are shown in **Figure S1 (a)** and **(b)** respectively which are validated with the help of DFT in the further section. The top 10 performing MOFs gave regenerability in the range of 77% to 80.96% as the adsorption sites can undergo reversible changes which can affect their ability to release adsorbed species completely. **Figure 5 (b)** shows that for the TSA conditions, the highest APS value obtained is only 95.55 mmol/g by Zr-DTDC MOF with a high CO_2/N_2 selectivity of 38.09 and ΔN_{CO2} of 2.51 mmol/g. The regenerability value of 78.49% is obtained by the same MOF. The least APS of 2.18 is obtained by the Zr_6-fBPDC which uses fluorinated biphenyl-4,4'dicarboxylate as the organic linker. Most of the MOFs gave APS values lower than 40 mmol/g which indicates that the TSA conditions are comparatively unsuitable for the post-combustion CO_2 capture with MOFs. **Figure 5 (c)** indicates the relation of regenerability and heat of adsorption with the variation of APS values. The optimum range of HOA is found in the range of 20 kJ/mol to 25 kJ/mol. MOF Zr-DTDC gave the HOA value of 23.83 kJ/mol which is found to be the most optimum interaction between MOF structure and CO_2 molecule. Either very low or very high HOA values resulted in the reduction of regenerability and APS values as well. The extremely low HOA resulted in the reduced interaction between the MOF and CO_2 molecule which decreases the gas uptake, while extremely high interaction results in the difficulty during the regeneration process. Similarly, from **Figure 5 (d)**, it can be anticipated that the optimum range of CO_2 HOA at 308K is found to be in the range of 20 to 25 kJ/mol. In this range, MOFs are easier to generate with a sufficient amount of CO_2-capturing ability.

Similarly, **Table 6** lists the top-performing MOFs for the TSA conditions. From this list, it is found that a total of 9 MOFs are found to be common for the VSA and TSA conditions. The top-performing MOF for the TSA is Zr-DTDC with the highest APS value of 95.55 mmol/g. The CO_2/N_2 selectivity for this MOF is 38.03 with a ΔN_{CO2} of 2.51 mmol/g. The regenerability value of 78.49% is provided by this MOF indicating the reduction of the number

of cycles during the TSA conditions. The MOF-804 is also found to be one of the top-performing MOFs. This MOF contains BPDC as an organic linker with each benzene ring having a carboxyl group at the para position, allowing it to coordinate with the Zr_6 clusters and form a 3D framework with surface area. MOFs such as Zr-DTDC are found to be ultrahigh thermally stable MOFs due to the joint action of the electronic effect and steric hindrance from methyl groups, as well as the Zr-O bond [64].

Table 4. Top performing MOFs for PSA.

MOF name	LCD (Å)	PLD (Å)	ρ (g/cm^3)	ASA (m^2/g)	VF	HOA (6 bar) (kJ/mol)	ΔN_{CO_2} (mmol/g)	S_{CO_2/N_2}	APS (mmol/g)	R (%)
MOF-525	16.26	4.26	0.69	3503.05	0.70	22.58	9.59	33.62	322.76	86.86
Zr-MTBC	14.54	8.01	0.58	4088.9	0.74	19.03	7.45	26.27	195.79	86.37
BUT-10	9.55	4.97	0.85	3292.5	0.68	23.69	7.19	26.66	191.87	76.63
MOF-806	12.79	5.93	0.78	3051.76	0.69	20.87	6.70	26.41	176.98	82.22
Zn-DPDBP-UiO	23.64	4.28	0.54	3889.36	0.74	19.04	6.98	25.14	175.52	83.97
UiO-67-Cl	12.55	6.16	0.79	3147.06	0.67	20.27	6.19	28.29	175.14	85.67
UiO-67-BN	11.03	5.26	0.91	1979.83	0.59	25.91	6.55	25.65	168.26	74.70
TBP-MOF-Cu	14.37	4.22	0.84	2635.76	0.62	23.33	6.49	25.72	167.09	76.26
Zr-CCA	9.92	5.33	0.87	3186.36	0.63	21.64	5.86	27.52	161.49	82.92
Zr-BTDC	10.84	5.95	0.91	2911.23	0.65	22.81	6.05	26.50	160.51	77.23

Table 5. Top performing MOFs for VSA.

MOF name	LCD (Å)	PLD (Å)	ρ (g/cm^3)	ASA (m^2/g)	VF	HOA (6 bar) (kJ/mol)	ΔN_{CO_2} (mmol/g)	S_{CO_2/N_2}	APS (mmol/g)	R (%)
MOF-805	9.22	4.80	1.03	2428.99	0.61	24.92	3.95	39.72	157.05	96.21
BUT-66	6.97	6.17	1.05	1932.03	0.52	27.79	4.50	33.35	150.43	94.51
Zr-TDC	9.80	5.22	1.08	2457.34	0.63	23.96	3.55	39.72	141.15	96.68
Zr-DTDC	8.42	4.02	1.17	1946.08	0.55	27.50	4.12	33.79	139.34	93.90
MOF-812	5.80	3.97	1.17	2044	0.43	27.63	3.33	39.10	130.36	94.69
BUT-67	7.96	6.29	0.92	2219.2	0.55	22.87	3.80	33.10	125.95	95.22
DUT-52	9.23	4.42	0.94	2936.55	0.60	23.00	3.18	39.27	125.08	96.94
BUT-11	10.25	4.93	0.90	3170.57	0.66	22.11	3.20	31.76	101.78	96.14
BUT-10	9.55	4.97	0.85	3292.5	0.68	20.90	3.09	32.36	100.33	96.65
TBP-MOF(Cu)	14.37	4.22	0.84	2635.76	0.61	21.37	2.84	31.77	90.26	96.27

Table 6. Top performing MOFs for TSA.

MOF name	LCD (Å)	PLD (Å)	ρ (g/cm^3)	ASA (m^2/g)	VF	HOA (6 bar) (kJ/mol)	ΔN_{CO2} (mmol/g)	$S_{CO2/N2}$	APS (mmol/g)	R (%)
Zr-DTDC	8.42	4.02	1.17	1946.08	0.55	23.83	2.51	38.03	95.55	78.49
BUT-66	6.97	6.17	1.05	1932.03	0.52	23.17	2.40	34.60	83.25	78.89
MOF-805	9.22	4.80	1.03	2428.99	0.61	21.12	2.12	38.98	82.69	80.96
MOF-812	5.80	3.97	1.17	2044	0.43	24.10	1.87	40.57	76.16	80.49
Zr-TDC	9.80	5.22	1.08	2457.34	0.63	20.18	1.73	35.01	60.88	80.35
DUT-52	9.23	4.42	0.94	2936.55	0.60	19.23	1.49	33.24	49.85	79.57
BUT-67	7.96	6.29	0.92	2219.2	0.55	21.07	1.71	28.56	49.09	77.61
BUT-11	10.25	4.93	0.90	3170.57	0.66	19.71	1.55	30.11	46.71	76.81
BUT-10	9.55	4.97	0.85	3292.5	0.68	18.73	1.45	29.88	43.45	76.90
MOF-804	7.76	3.54	1.36	1669.31	0.49	24.28	1.47	28.6	42.08	73.07

3.2.2 Structure-performance relationships

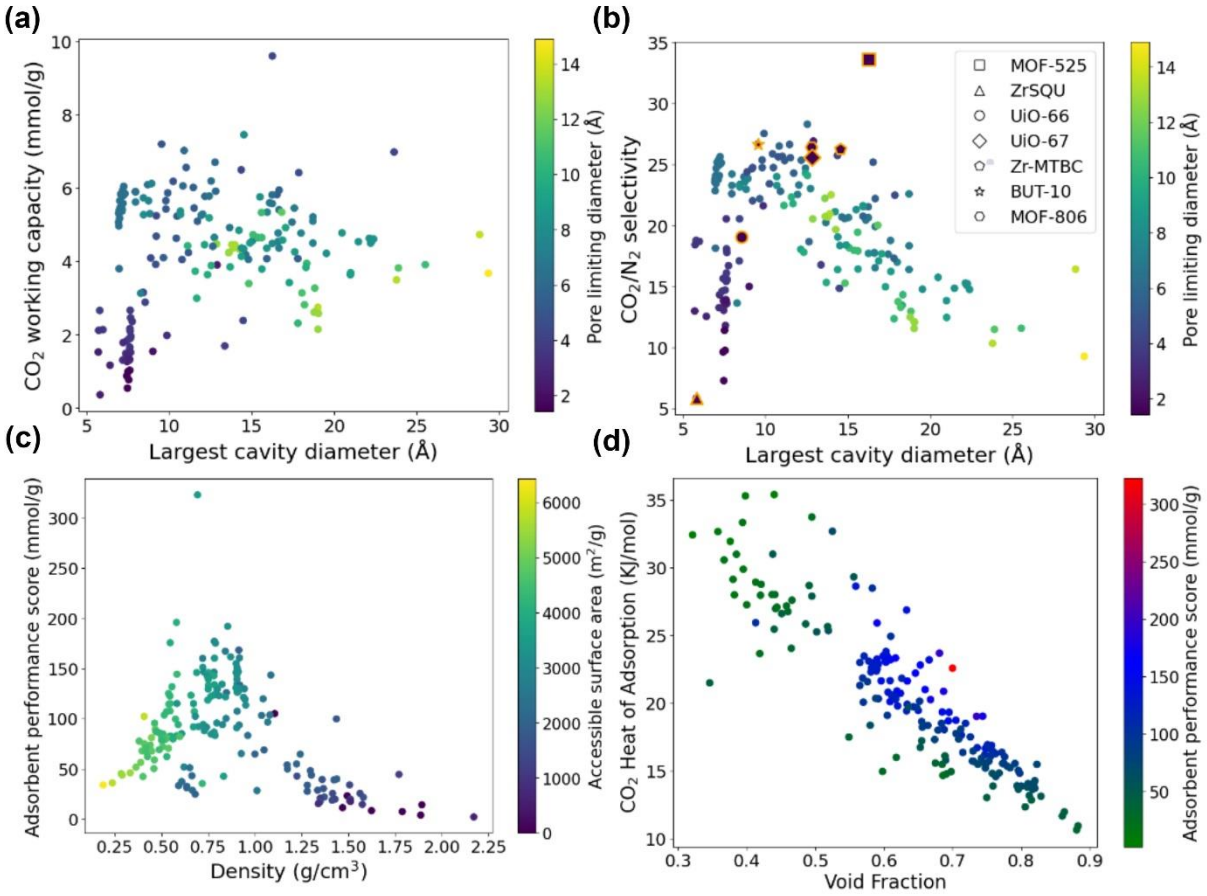

Figure 6. Structure relationship plots for the PSA condition (a) ΔN_{CO2} v/s LCD, (b) CO_2/N_2 selectivity v/s LCD, (c) APS v/s Density, and (d) CO_2 heat of adsorption v/s VF.

The structure-property relationship for all 3 adsorption conditions is performed as visualized in **Figures 6**, **7**, and **8**. Different geometrical properties such as largest cavity diameter, pore limiting diameter, density, and accessible surface area are chosen for the analysis. This relationship helps researchers optimize these geometrical features for maximizing the CO_2 capacity. The kinetics of CO_2 adsorption are also highly reliable regarding the structural arrangement and presence of functional groups on the MOF structures. Understanding the structural impact on diffusion and adsorption rates of CO_2 can lead to the development of MOFs with improved adsorption and regeneration. **Figure 6 (a)** indicates the relationship between ΔN_{CO2} and LCD with the variation of PLD. It shows that the low PLD and LCD are unfavorable for capturing CO_2 molecules due to reduced adsorption capacity as

small pore sizes can limit the amount of CO_2 adsorbed by the MOFs. Lower PLD can restrict the entrance of CO_2 molecules, resulting in less CO_2 adsorption. Also, lower LCD values reduce the availability of space inside the MOF structure for CO_2 molecules, thus reducing the interaction sites [65]. It is observed in the plot that at lower values of PLD and LCD, the CO_2 capacity is found to be lower than 3 mmol/g. However, higher LCD values are also found to be unfavorable as it leads to weaker molecular interaction. A significant portion of the surface area also goes unutilized which might result in the increased capturing of N_2 molecules over CO_2. Similar trends are also observed for the selectivity of CO_2/N_2 for all 182 Zr-based MOFs as shown in **Figure 6 (b)**. From the plot, it can be observed that with the increase in LCD or PLD, CO_2/N_2 selectivity initially increases rapidly and then drops, since a high value of LCD or PLD can lead to weaker interactions which are not preferential for selective adsorption. Therefore, it can be concluded that efficient CO_2 capture in MOFs typically requires optimum balance for the LCD, PLD, and accessible surface area of MOFs for efficient gas transportation [66]. From the generated plots, the optimum range is found to be in the range of 9.55 Å to 16.26 Å for the LCD and 4.22 Å to 8.01 Å for the PLD. The detailed structure-property is also carried out by understanding the relationship between the APS and density of Zr-MOFs with the variation of accessible surface area of MOFs. The extremely low-density MOFs are prone to collapse under various environmental stresses which can lead to loss in porosity and active sites necessary for CO_2 adsorption. Apart from that, when a MOF has low density, its reduced number of Zinc metal sites or functional groups can limit the interaction available for the CO_2 molecules. Therefore, low-dense adsorbents become less efficient in capturing CO_2 compared to higher-dense adsorbents [67]. However, extremely high-dense MOFs are also possessed with small pore volumes, affecting gas accessibility. This restriction can stop CO_2 molecules from entering the effectively, making it difficult to interact with MOFs. The optimum range

for the density is found to be 0.54 g/cm^3 to 0.91 g/cm^3 with a higher accessible surface area of more than 2500 m^2/g.

Figure 6 (d) shows the interaction of CO_2 HOA with the void fraction of MOFs with the variation of APS. It can be found that higher values of VF result in more unoccupied volume with the MOF. Therefore, the increase in VF results in the effective reduction in the surface area available to the CO_2 molecule to interact with functional groups and adsorption sites. At an optimum value of VF, the MOF materials tend to show high APS with minimal HOA. The optimum range for the VF is found to be between 0.5 and 0.65. Therefore, understanding the optimum range of the geometrical features aids in the designing best suitable MOFs. For the

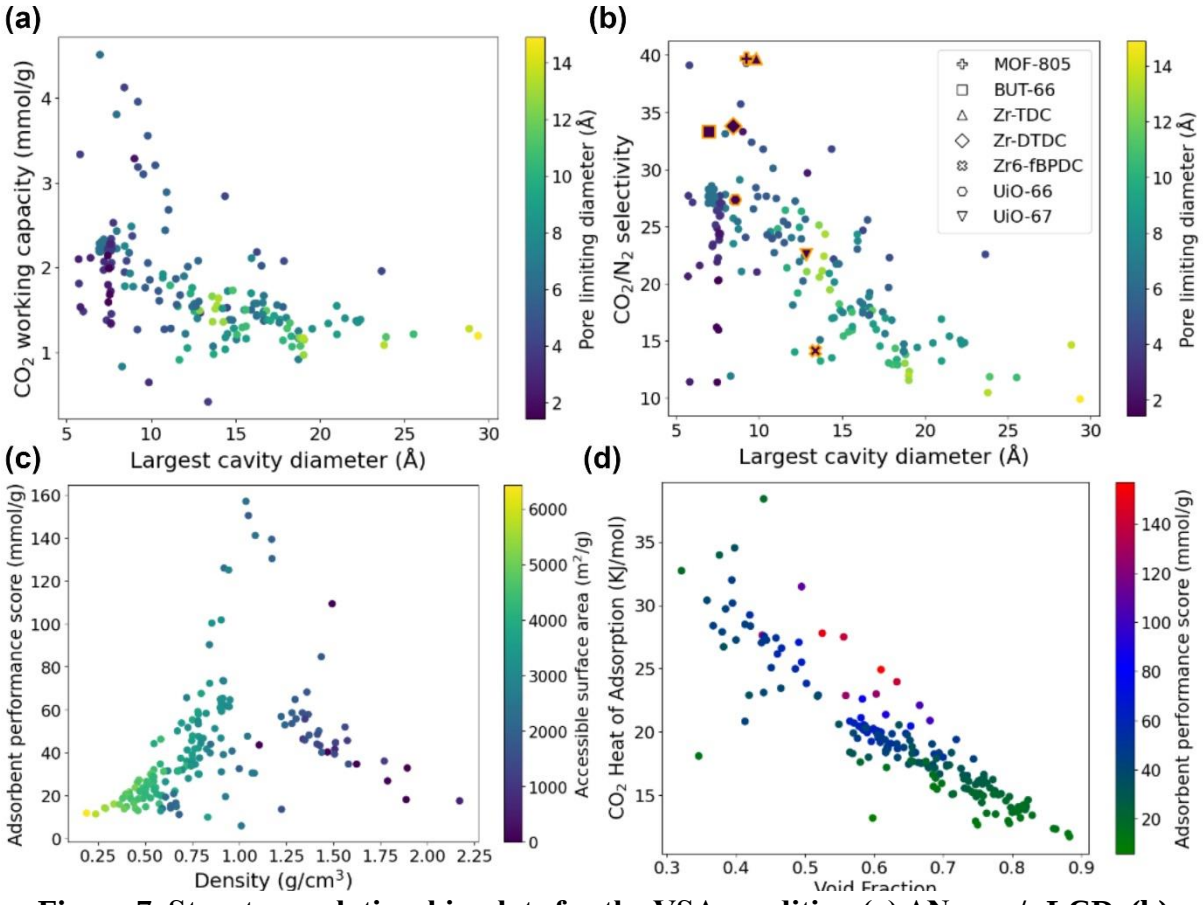

Figure 7. Structure relationship plots for the VSA condition (a) ΔN_{CO2} v/s LCD, (b) CO_2/N_2 selectivity v/s LCD, (c) APS v/s Density, and (d) CO_2 heat of adsorption v/s VF.

PSA condition, the optimum range is found to be 9.55 Å < LCD < 16.26 Å, 4.22 Å < PLD < 8.01 Å, 0.54 g/cm^3 < density < 0.91 g/cm^3, 0.59 < void fraction < 0.74.

Figures 7 and **8** show multiple structure-property plots for the VSA and TSA conditions for the Zr-based MOFs. Similar patterns in the plots are observed for the PSA, VSA, and TSA conditions, however, some notable key points are observed from the developed plot for both VSA and TSA simulations. The PSA condition involves high-pressure-induced gas adsorption. If the MOF has an appropriate pore diameter, it can effectively adsorb target gas at high pressure. High PLD and LCD are favorable for the PSA conditions as they can facilitate faster kinetics for gas uptakes during high-pressure adsorption phases [68]. However, VSA relies on desorption with the help of vacuum pressure conditions. Therefore, smaller and narrower pores can be useful to increase the CO_2 selectivity over N_2 gas molecules. Similarly, TSA depends on the temperature variation for the efficient separation of CO_2 gas. Therefore, the optimum range for the VSA and TSA conditions varies a bit compared to the PSA conditions. The optimum range of various geometrical features for the VSA is 5.88 Å < LCD < 10.25 Å, 3.97 Å < PLD < 6.29 Å, 0.84 g/cm^3 < density < 1.17 g/cm^3, 0.52 < void fraction < 0.68. For the TSA condition, the optimum range is found to be 5.88 Å < LCD < 10.25 Å, 3.54 Å < PLD < 6.29 Å, 0.9 g/cm^3 < density < 1.36 g/cm^3, 0.49 < void fraction < 0.68. Most of the optimum

range for the VSA and TSA lies in the same order as 9 top-performing MOFs for VSA and TSA are found to be similar.

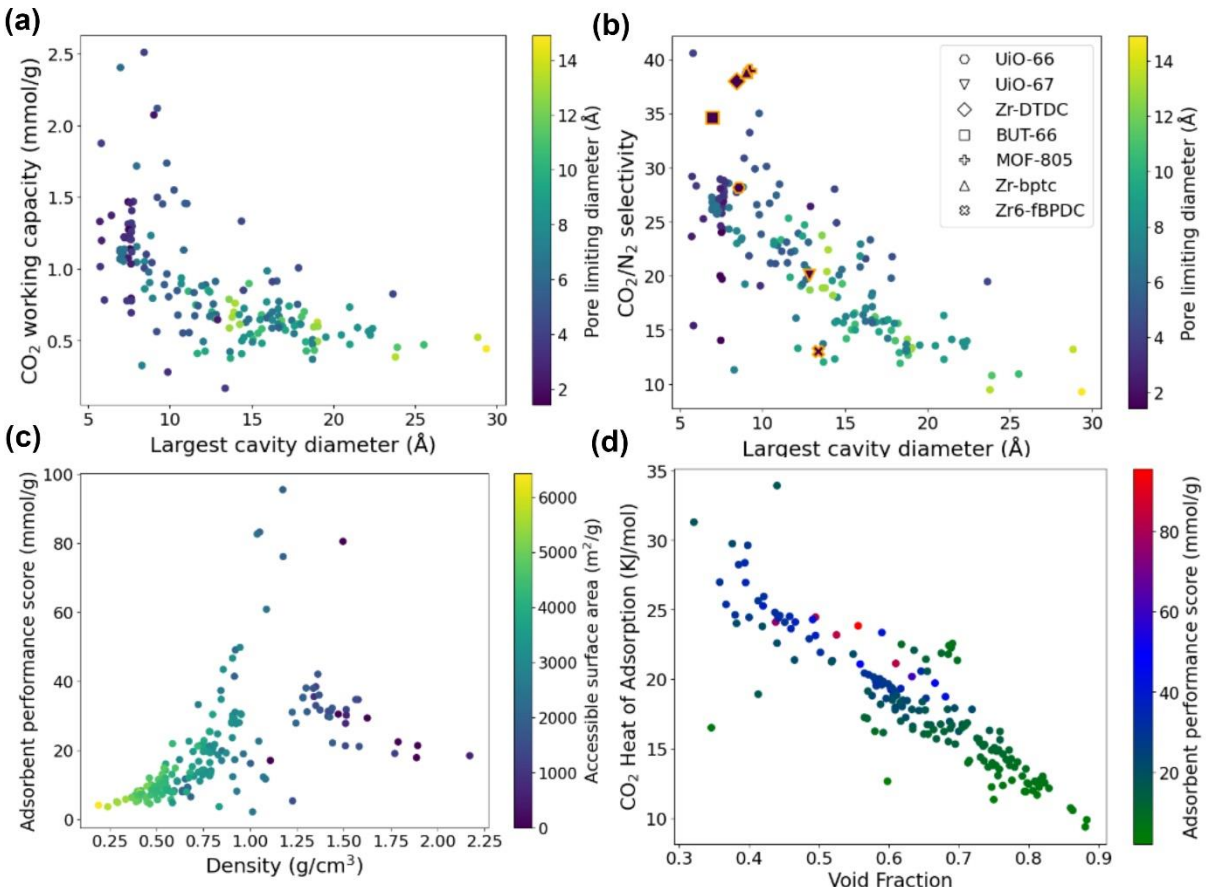

Figure 8. Structure relationship plots for the TSA condition (a) ΔN_{CO2} v/s LCD, (b) CO_2/N_2 selectivity v/s LCD, (c) APS v/s Density, and (d) CO_2 heat of adsorption v/s VF.

3.3 Density functional theory calculation of CO_2 and N_2 adsorption on MOF-805

Table 7. CO_2 adsorption active sites thermodynamics on the MOF-805.

CO_2 adsorption on MOF-805						
Active site	**Site 1**	**Site 2**	**Site 3**	**Site 4**	**Site 5**	**Site 6**
Binding Energy	-9.01	-19.95	-21.63	-27.89	-26.77	-22.83
Enthalpy/Heat of adsorption (kJ/mol)	-8.16	-19.95	-21.63	-27.89	-26.77	-22.83

Table 8. N_2 adsorption active sites thermodynamics on the MOF-805.

N_2 adsorption on MOF-805				
Active site	Site 1	Site 2	Site 3	Site 4
Binding Energy	-13.79	-13.74	-15.64	-15.64
Enthalpy/Heat of adsorption (kJ/mol)	-12.94	-13.74	-15.64	-15.64

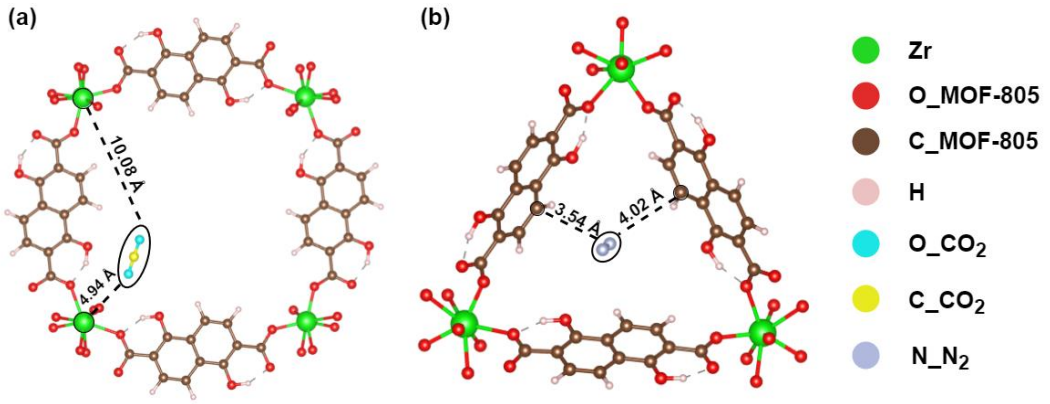

Figure 9. Strongest binding sites of MOF-805 for (a) CO_2 near metal and (b) N_2 near the linker.

Tables 7 and **8** show the binding energy and heat of adsorptions calculated from **Equations 1** and **2** for the CO_2 and N_2 adsorption sites on the MOF-805. Site 4 where the CO_2 molecule is located close to the metal atom, was found to be a strong binding site with an adsorption energy of -27.89 kJ/mol. The three-ringed and four-ringed structures (refer to **Figure S2 (a)** and **(b)**) for the MOF-805 with the strongest adsorption sites of CO_2 and N_2 are visualized in **Figure 9 (a)** and **(b)** respectively. The nearest distance for the CO_2 is 4.94 Å with the metal ion, while the closest distance for the N_2 molecule from the linker is 3.54 Å. The CO_2

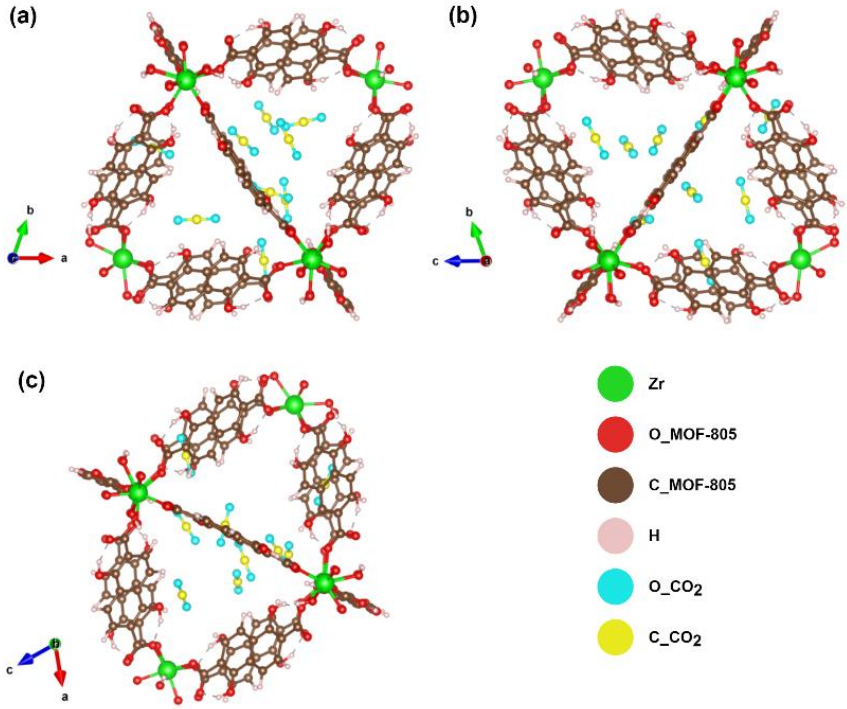

Figure 10. Crystal structure of MOF-805 with the adsorption of 9 CO_2 molecules, (a) Front View, (b) Side View, and (c) Top View.

at the center is the weakest adsorption site with energy -8.16 kJ/mol which can be observed from **Figure S3 (a)** to **(f)** showing the presence of CO_2 gas molecules at 6 different sites of the MOF-805. The horizontal and vertical distance of the CO_2 near the metal center is found to be 4.94 Å and 4.92 Å respectively. In contrast, the optimized distance of the CO_2 molecule from the linker is 3.92 Å. The preferential adsorption sites of CO_2 on MOF-805 are as follows Site 4 (i.e., -27.89 kJ/mol)> Site 5 (i.e., -26.77 kJ/mol) > Site 6 (i.e., -22.83) > Site 3 (i.e., -21.63 kJ/mol) > Site 2 (i.e., -19.95 kJ/mol) > Site 1 (i.e., -8.16 kJ/mol). The CO_2 molecules are populated in the 9 active sites of the MOF-805 framework according to the preferential sites visualized in **Figure 10 (a)** to **(c)**. The adsorption energy obtained is -24.34 kJ/mol which is close to the CO_2 heat of adsorption estimated by GCMC i.e. -24.92 kJ/mol. The strongest N_2 adsorption site on the framework is Site 4, located near the metal and linker of the MOF 805 as shown in **Figure S4 (a)** to **(d)** also shows the crystal structure of the N_2 molecule near horizontal and vertical windows and the N_2 molecule at the center of MOF-805. The distance between the N_2 molecule near the linker is 3.29 Å. The preferential adsorption sites of nitrogen are site 4 (i.e., -15.64 kJ/mol) = Site 3 (i.e., -15.64 kJ/mol) > Site 2 (i.e., -13.74 kJ/mol) > Site 1 (i.e., -12.94 kJ/mol). The adsorption energy obtained is -15.64 kJ/mol which is close to the N_2 heat of adsorption estimated by GCMC i.e. -13.34 kJ/mol.

4. Conclusion

We have conducted a computational screening of the 182 Zr-MOFs for PSA, VSA, and TSA conditions of the CO_2/N_2 separation. Comprehensive theoretical analysis and estimation of the physical, chemical, and adsorption characteristics are crucial for understanding the carbon capture behavior on Zr-MOFs. Our simulations predicted the MOF-525, MOF-805, and Zr-DTDC MOFs as the top-performing MOFs for the PSA, VSA, and TSA respectively. These MOFs gave the highest adsorbent performance score values of 322 mmol/g, 157 mmol/g, and 95.5 mmol/g corresponding to PSA, VSA, and TSA conditions. The top 10 MOFs were ranked

according to their theoretical performance for three respective conditions. The presence of a carboxyl group on the organic linkers enhanced π-π interactions with polar gases, especially CO_2 which results in better adsorption. Similarly, a structure-property relationship was performed with the variation of different structural parameters such as void fraction, gravimetric surface area, pore limiting diameter, largest cavity diameter, and density. The optimum range for the efficient CO_2/N_2 selectivity for all three conditions was identified. For the PSA condition, 9.55 Å < LCD < 16.26 Å, 4.22 Å < PLD < 8.01 Å, 0.54 g/cm^3 < density < 0.91 g/cm^3, 0.59 < void fraction < 0.74. For the VSA condition is 5.88 Å < LCD < 10.25 Å, 3.97 Å < PLD < 6.29 Å, 0.84 g/cm^3 < density < 1.17 g/cm^3, 0.52 < void fraction < 0.68. Similarly, for the TSA condition, the optimum range is found to be 5.88 Å < LCD < 10.25 Å, 3.54 Å < PLD < 6.29 Å, 0.9 g/cm^3 < density < 1.36 g/cm^3, 0.49 < void fraction < 0.68. The DFT calculations were performed for the top-performing framework of VSA simulation, i.e., MOF-805. From the DFT study, preferential adsorption sites of CO_2 on MOF-805 were discovered as follows Site 4 (i.e., -27.89 kJ/mol)> Site 5 (i.e., -26.77 kJ/mol) > Site 6 (i.e., -22.83) > Site 3 (i.e., -21.63 kJ/mol) > Site 2 (i.e., -19.95 kJ/mol) > Site 1 (i.e., -8.16 kJ/mol). The adsorption energy estimated for the complete saturation of the CO_2 molecules in the MOF-805 framework is -24.34 kJ/mol. DFT analysis provides a deep understanding of the adsorption behavior of the CO_2 and N_2 molecules on the Zr-based MOF structures.

Acknowledgment

The authors sincerely thank the Indian Institute of Petroleum & Energy Visakhapatnam for providing access to its research facilities and resources. Their invaluable support and infrastructure played a crucial role in the successful completion of this study.

References

[1] Jeffry L, Ong MY, Nomanbhay S, Mofijur M, Mubashir M, Show PL. Greenhouse gases utilization: A review. Fuel 2021;301. https://doi.org/10.1016/j.fuel.2021.121017.

[2] Lucas PL, van Vuuren DP, Olivier JGJ, den Elzen MGJ. Long-term reduction potential of non-CO2 greenhouse gases. Environ Sci Policy 2007;10:85–103. https://doi.org/10.1016/j.envsci.2006.10.007.

[3] Kattel S, Liu P, Chen JG. Tuning Selectivity of CO2 Hydrogenation Reactions at the Metal/Oxide Interface. J Am Chem Soc 2017;139:9739–54. https://doi.org/10.1021/jacs.7b05362.

[4] Ploetz E, Engelke H, Lächelt U, Wuttke S. The Chemistry of Reticular Framework Nanoparticles: MOF, ZIF, and COF Materials. Adv Funct Mater 2020;30. https://doi.org/10.1002/adfm.201909062.

[5] Zheng B, Huang L, Cao X, Shen S, Cao H, Hang C, et al. A highly porous acylamide decorated MOF-505 analogue exhibiting high and selective CO2 gas uptake capability. CrystEngComm 2018;20:1874–81. https://doi.org/10.1039/c8ce00103k.

[6] Sava Gallis DF, Harvey JA, Pearce CJ, Hall MG, DeCoste JB, Kinnan MK, et al. Efficient MOF-based degradation of organophosphorus compounds in non-aqueous environments. J Mater Chem A Mater 2018;6:3038–45. https://doi.org/10.1039/c7ta10794c.

[7] Erucar I, Keskin S. Computational assessment of MOF membranes for CH4/H2 separations. J Memb Sci 2016;514:313–21. https://doi.org/10.1016/j.memsci.2016.04.070.

[8] Wilmer CE, Snurr RQ. Towards rapid computational screening of metal-organic frameworks for carbon dioxide capture: Calculation of framework charges via charge equilibration. Chemical Engineering Journal 2011;171:775–81. https://doi.org/10.1016/j.cej.2010.10.035.

[9] Chung YG, Haldoupis E, Bucior BJ, Haranczyk M, Lee S, Zhang H, et al. Advances, Updates, and Analytics for the Computation-Ready, Experimental Metal-Organic Framework Database: CoRE MOF 2019. J Chem Eng Data 2019;64:5985–98. https://doi.org/10.1021/acs.jced.9b00835.

[10] Boyd PG, Chidambaram A, García-Díez E, Ireland CP, Daff TD, Bounds R, et al. Data-driven design of metal–organic frameworks for wet flue gas CO2 capture. Nature 2019;576:253–6. https://doi.org/10.1038/s41586-019-1798-7.

[11] Colón YJ, Gómez-Gualdrón DA, Snurr RQ. Topologically Guided, Automated Construction of Metal–Organic Frameworks and Their Evaluation for Energy-Related Applications. Cryst Growth Des 2017;17:5801–10. https://doi.org/10.1021/acs.cgd.7b00848.

[12] Yin X, Gounaris CE. Computational discovery of Metal–Organic Frameworks for sustainable energy systems: Open challenges. Comput Chem Eng 2022;167:108022. https://doi.org/10.1016/j.compchemeng.2022.108022.

[13] Duan J, Jin W, Kitagawa S. Water-resistant porous coordination polymers for gas separation. Coord Chem Rev 2017;332:48–74. https://doi.org/10.1016/j.ccr.2016.11.004.

[14] Bai Y, Dou Y, Xie LH, Rutledge W, Li JR, Zhou HC. Zr-based metal-organic frameworks: Design, synthesis, structure, and applications. Chem Soc Rev 2016;45:2327–67. https://doi.org/10.1039/c5cs00837a.

[15] Cavka JH, Jakobsen S, Olsbye U, Guillou N, Lamberti C, Bordiga S, et al. A new zirconium inorganic building brick forming metal organic frameworks with exceptional stability. J Am Chem Soc 2008;130:13850–1. https://doi.org/10.1021/ja8057953.

[16] Yang Q, Vaesen S, Ragon F, Wiersum AD, Wu D, Lago A, et al. A water stable metal-organic framework with optimal features for CO 2 capture. Angewandte Chemie - International Edition 2013;52:10316–20. https://doi.org/10.1002/anie.201302682.

[17] Schaate A, Roy P, Preuße T, Lohmeier SJ, Godt A, Behrens P. Porous interpenetrated zirconium-organic frameworks (PIZOFs): A chemically versatile family of metal-organic frameworks. Chemistry - A European Journal 2011;17:9320–5. https://doi.org/10.1002/chem.201101015.

[18] Zhang X, Zhang X, Johnson JA, Chen YS, Zhang J. Highly Porous Zirconium Metal-Organic Frameworks with β-UH3-like Topology Based on Elongated Tetrahedral Linkers. J Am Chem Soc 2016;138:8380–3. https://doi.org/10.1021/jacs.6b04608.

[19] Bezrukov AA, Törnroos KW, Le Roux E, Dietzel PDC. Incorporation of an intact dimeric Zr12 oxo cluster from a molecular precursor in a new zirconium metal-organic framework. Chemical Communications 2018;54:2735–8. https://doi.org/10.1039/c8cc00507a.

[20] Bon V, Senkovska I, Weiss MS, Kaskel S. Tailoring of network dimensionality and porosity adjustment in Zr- and Hf-based MOFs. CrystEngComm 2013;15:9572–7. https://doi.org/10.1039/c3ce41121d.

[21] Feng D, Jiang HL, Chen YP, Gu ZY, Wei Z, Zhou HC. Metal-organic frameworks based on previously unknown Zr8/Hf 8 cubic clusters. Inorg Chem 2013;52:12661–7. https://doi.org/10.1021/ic4018536.

[22] Gao J, Huang C, Lin Y, Tong P, Zhang L. In situ solvothermal synthesis of metal-organic framework coated fiber for highly sensitive solid-phase microextraction of polycyclic aromatic hydrocarbons. J Chromatogr A 2016;1436:1–8. https://doi.org/10.1016/j.chroma.2016.01.051.

[23] Si T, Ma J, Lu X, Wang L, Liang X, Wang S. Core-Shell Metal-Organic Frameworks as the Stationary Phase for Hydrophilic Interaction Liquid Chromatography. ACS Appl Nano Mater 2020;3:351–6. https://doi.org/10.1021/acsanm.9b01987.

[24] Wang TC, Bury W, Gómez-Gualdrón DA, Vermeulen NA, Mondloch JE, Deria P, et al. Ultrahigh Surface Area Zirconium MOFs and Insights into the Applicability of the BET Theory. J Am Chem Soc 2015;137:3585–91. https://doi.org/10.1021/ja512973b.

[25] Zhang HT, Zhang JW, Huang G, Du ZY, Jiang HL. An amine-functionalized metal–organic framework as a sensing platform for DNA detection. Chemical Communications 2014;50:12069–72. https://doi.org/10.1039/c4cc05571c.

[26] Chen M, Gan N, Zhou Y, Li T, Xu Q, Cao Y, et al. A novel aptamer- metal ions- nanoscale MOF based electrochemical biocodes for multiple antibiotics detection and signal amplification. Sens Actuators B Chem 2017;242:1201–9. https://doi.org/10.1016/j.snb.2016.08.185.

[27] Hao JN, Yan B. A water-stable lanthanide-functionalized MOF as a highly selective and sensitive fluorescent probe for Cd2+. Chemical Communications 2015;51:7737–40. https://doi.org/10.1039/c5cc01430a.

[28] Moghaddam ZS, Kaykhaii M, Khajeh M, Oveisi AR. Synthesis of UiO-66-OH zirconium metal-organic framework and its application for selective extraction and trace determination of thorium in water samples by spectrophotometry. Spectrochim Acta A Mol Biomol Spectrosc 2018;194:76–82. https://doi.org/10.1016/j.saa.2018.01.010.

[29] Shan B, McIntyre SM, Armstrong MR, Shen Y, Mu B. Investigation of Missing-Cluster Defects in UiO-66 and Ferrocene Deposition into Defect-Induced Cavities. Ind Eng Chem Res 2018;57:14233–41. https://doi.org/10.1021/acs.iecr.8b03516.

[30] Gomez-Gualdron DA, Gutov O V., Krungleviciute V, Borah B, Mondloch JE, Hupp JT, et al. Computational design of metal-organic frameworks based on stable zirconium building units for storage and delivery of methane. Chemistry of Materials 2014;26:5632–9. https://doi.org/10.1021/cm502304e.

[31] Zhou F, Zheng B, Liu D, Wang Z, Yang Q. Large-Scale Structural Refinement and Screening of Zirconium Metal-Organic Frameworks for H2S/CH4 Separation. ACS Appl Mater Interfaces 2019;11:46984–92. https://doi.org/10.1021/acsami.9b17885.

[32] Oktavian R, Schireman R, Glasby LT, Huang G, Zanca F, Fairen-Jimenez D, et al. Computational Characterization of Zr-Oxide MOFs for Adsorption Applications. ACS Appl Mater Interfaces 2022;14:56938–47. https://doi.org/10.1021/acsami.2c13391.

[33] Qi H, Xu Y, Gu N, Han Y, Zhang X, Zeng Y. High-Throughput Computational Screening of Experimental Zr-Based MOFs for Elemental Mercury Capture. Ind Eng Chem Res 2023;62:14497–506. https://doi.org/10.1021/acs.iecr.3c01182.

[34] Bureekaew S, Schmid R. Hypothetical 3D-periodic covalent organic frameworks: Exploring the possibilities by a first principles derived force field. CrystEngComm 2013;15:1551–62. https://doi.org/10.1039/c2ce26473k.

[35] Dubbeldam D, Calero S, Ellis DE, Snurr RQ. RASPA: Molecular simulation software for adsorption and diffusion in flexible nanoporous materials. Mol Simul 2016;42:81–101. https://doi.org/10.1080/08927022.2015.1010082.

[36] Willems TF, Rycroft CH, Kazi M, Meza JC, Haranczyk M. Algorithms and tools for high-throughput geometry-based analysis of crystalline porous materials. Microporous and Mesoporous Materials 2012;149:134–41. https://doi.org/10.1016/j.micromeso.2011.08.020.

[37] Avci G, Erucar I, Keskin S. Do New MOFs Perform Better for CO_2 Capture and H_2 Purification? Computational Screening of the Updated MOF Database. ACS Appl Mater Interfaces 2020;12:41567–79. https://doi.org/10.1021/acsami.0c12330.

[38] Yang MW, Chen NC, Huang CH, Shen YT, Yang HS, Chou CT. Temperature swing adsorption process for CO2 capture using polyaniline solid sorbent. Energy Procedia, vol. 63, Elsevier Ltd; 2014, p. 2351–8. https://doi.org/10.1016/j.egypro.2014.11.256.

[39] Harris JG, Yungt KH. Carbon Dioxide's Liquid-Vapor Coexistence Curve and Critical Properties As Predicted by a Simple Molecular Model. vol. 99. 1995.

[40] Potoff JJ, Siepmann JI. Vapor–liquid equilibria of mixtures containing alkanes, carbon dioxide, and nitrogen. AIChE Journal 2001;47:1676–82. https://doi.org/10.1002/aic.690470719.

[41] Rappe AK, Casewit CJ, Colwell KS, Goddard WA, Skiff WM. UFF, a full periodic table force field for molecular mechanics and molecular dynamics simulations. J Am Chem Soc 1992;114:10024–35. https://doi.org/10.1021/ja00051a040.

[42] Cheng M, Wang S, Zhang Z, Ji X, Liu C, Dai Y, et al. High-throughput virtual screening of metal–organic frameworks for xenon recovery from exhaled anesthetic gas mixture. Chemical Engineering Journal 2023;451. https://doi.org/10.1016/j.cej.2022.138218.

[43] Kresse G, Hafner J. *Ab initio* molecular dynamics for liquid metals. Phys Rev B 1993;47:558–61. https://doi.org/10.1103/PhysRevB.47.558.

[44] Kresse G, Furthmüller J. Efficiency of ab-initio total energy calculations for metals and semiconductors using a plane-wave basis set. Comput Mater Sci 1996;6:15–50. https://doi.org/10.1016/0927-0256(96)00008-0.

[45] Kresse G, Furthmüller J. Efficient iterative schemes for *ab initio* total-energy calculations using a plane-wave basis set. Phys Rev B 1996;54:11169–86. https://doi.org/10.1103/PhysRevB.54.11169.

[46] Kresse G, Joubert D. From ultrasoft pseudopotentials to the projector augmented-wave method. Phys Rev B 1999;59:1758–75. https://doi.org/10.1103/PhysRevB.59.1758.

[47] Blöchl PE. Projector augmented-wave method. Phys Rev B 1994;50:17953–79. https://doi.org/10.1103/PhysRevB.50.17953.

[48] Ernzerhof M, Scuseria GE. Assessment of the Perdew–Burke–Ernzerhof exchange-correlation functional. J Chem Phys 1999;110:5029–36. https://doi.org/10.1063/1.478401.

[49] Schröder H, Creon A, Schwabe T. Reformulation of the D3(Becke–Johnson) Dispersion Correction without Resorting to Higher than C_6 Dispersion Coefficients. J Chem Theory Comput 2015;11:3163–70. https://doi.org/10.1021/acs.jctc.5b00400.

[50] Allen FH. The Cambridge Structural Database: a quarter of a million crystal structures and rising. Acta Crystallogr B 2002;58:380–8. https://doi.org/10.1107/S0108768102003890.

[51] Chung YG, Gómez-Gualdrón DA, Li P, Leperi KT, Deria P, Zhang H, et al. In silico discovery of metal-organic frameworks for precombustion CO2 capture using a genetic algorithm. Sci Adv 2016;2. https://doi.org/10.1126/sciadv.1600909.

[52] Cmarik GE, Kim M, Cohen SM, Walton KS. Tuning the adsorption properties of uio-66 via ligand functionalization. Langmuir 2012;28:15606–13. https://doi.org/10.1021/la3035352.

[53] Xu H, Mguni LL, Shan Y, Jewell LL, Hildebrandt D, Yao Y, et al. Computational prediction of MOFs with the potential to improve the efficiency of industrial CO2 capture. Sep Purif Technol 2025;354. https://doi.org/10.1016/j.seppur.2024.128927.

[54] Luo JP, Zhang J, Yin N, Wang TP, Tan ZC, Han W, et al. An experimental strategy for evaluating the energy performance of metal–organic framework-based carbon dioxide adsorbents. Chemical Engineering Journal 2022;442. https://doi.org/10.1016/j.cej.2022.136210.

[55] Soubeyrand-Lenoir E, Vagner C, Yoon JW, Bazin P, Ragon F, Hwang YK, et al. How water fosters a remarkable 5-fold increase in low-pressure CO 2 uptake within mesoporous MIL-100(Fe). J Am Chem Soc 2012;134:10174–81. https://doi.org/10.1021/ja302787x.

[56] Chen J, Wang G, Dong Y, Ji J, Li L, Xue M, et al. Controlling the Polarity of Metal–Organic Frameworks to Promote Electrochemical CO_2 Reduction. Angewandte Chemie International Edition 2024. https://doi.org/10.1002/anie.202416367.

[57] Wu X, Chen L, Amigues EJ, Wang R, Pang Z, Ding L. In Silico Tuning of the Pore Surface Functionality in Al-MOFs for Trace CH3I Capture. ACS Omega 2021;6:18169–77. https://doi.org/10.1021/acsomega.1c02072.

[58] AL-SAEDI RWM. A review on modified MOFs as CO2 adsorbents using mixed metals and functionalized linkers. Samarra Journal of Pure and Applied Science 2023;5:1–18. https://doi.org/10.54153/sjpas.2023.v5i1.428.

[59] Koschnick C, Terban MW, Frison R, Etter M, Böhm FA, Proserpio DM, et al. Unlocking New Topologies in Zr-Based Metal-Organic Frameworks by Combining Linker Flexibility and Building Block Disorder. J Am Chem Soc 2023;145:10051–60. https://doi.org/10.1021/jacs.2c13731.

[60] Wang L, Li T, Dong X, Pang M, Xiao S, Zhang W. Thiophene-based MOFs for iodine capture: Effect of pore structures and interaction mechanism. Chemical Engineering Journal 2021;425. https://doi.org/10.1016/j.cej.2021.130578.

[61] Bolotov VA, Kovalenko KA, Samsonenko DG, Han X, Zhang X, Smith GL, et al. Enhancement of CO2 Uptake and Selectivity in a Metal-Organic Framework by the Incorporation of Thiophene Functionality. Inorg Chem 2018;57:5074–82. https://doi.org/10.1021/acs.inorgchem.8b00138.

[62] Lyu H, Chen OIF, Hanikel N, Hossain MI, Flaig RW, Pei X, et al. Carbon Dioxide Capture Chemistry of Amino Acid Functionalized Metal-Organic Frameworks in Humid Flue Gas. J Am Chem Soc 2022;144:2387–96. https://doi.org/10.1021/jacs.1c13368.

[63] Parkar S, Mulukh R, Narhari G, Kulkarni S. Intensification of Temperature Swing Adsorption. Journal of Sustainable Materials Processing and Management 2022;2. https://doi.org/10.30880/jsmpm.2022.02.01.009.

[64] Bai Y, Dou Y, Xie LH, Rutledge W, Li JR, Zhou HC. Zr-based metal-organic frameworks: Design, synthesis, structure, and applications. Chem Soc Rev 2016;45:2327–67. https://doi.org/10.1039/c5cs00837a.

[65] Heydari-Gorji A, Yang Y, Sayari A. Effect of the pore length on CO2 adsorption over amine-modified mesoporous silicas. Energy and Fuels 2011;25:4206–10. https://doi.org/10.1021/ef200765f.

[66] Zhang Z, Zhao Y, Gong Q, Lib Z, Li J. MOFs for CO2 capture and separation from flue gas mixtures: The effect of multifunctional sites on their adsorption capacity and selectivity. Chemical Communications 2013;49:653–61. https://doi.org/10.1039/c2cc35561b.

[67] Ghanbari T, Abnisa F, Wan Daud WMA. A review on production of metal organic frameworks (MOF) for CO2 adsorption. Science of the Total Environment 2020;707. https://doi.org/10.1016/j.scitotenv.2019.135090.

[68] Hu P, Hu J, Wang H, Liu H, Zhou J, Liu Y, et al. One-Step Ethylene Purification by an Ethane-Screening Metal-Organic Framework. ACS Appl Mater Interfaces 2022;14:15195–204. https://doi.org/10.1021/acsami.1c25005.

Cover Letter

10/03/2025

To
The Editor
Energy
Elservier

Dear Respected Editor,

We would like to submit our research work entitled "**Computational discovery of the Zr based Metal organic frameworks for carbon dioxide capture**", authored by Iradat Hussain Mafat and Dr Sridhar Palla for the "Energy". We have worked in gas storage and separation in metal-organic frameworks for the past ten years and published several research articles in internationally recognised journals. Our recent article titled "Chemical-guided screening of top-performing metal-organic frameworks for hydrogen storage: An explainable deep attention convolutional model" was also discussed the discovery of the optimal hydrogen storage material by explainable artificial intelligence.

Zirconium based Metal-organic frameworks (MOFs) are highly innovative porous materials known for their exceptional gas storage capacity and gas selectivity. However, experimental synthesis and testing the carbon capture with multiple trial and errors of the ~182 Zr-MOFs is time consuming and expensive. Therefore in this article we provided a solution to identify top performing Zr-MOF for adsorption swing techniques by their performance metrics (i.e., physical, chemical and adsorption characteristics) by molecular simulations tools. This article recommends top performing Zr-MOF for the carbon capture application under Pressure Swing Adsorption (PSA), Temperature Swing Adsorption (TSA) and Vacuum Swing Adsorption (VSA) conditions.

All the authors have approved the manuscript and agreed with the submission to your esteemed 'Energy' jourrnal. The manuscript is original and has not been submitted for publication in any journal.

Thank You.

Dr. Sridhar Palla
Dept. of Chemical Engineering
Indian Institute of Petroleum and Energy Visakhapatnam
Visakhapatnam, India

Declaration of interests

☒The authors declare that they have no known competing financial interests or personal relationships that could have appeared to influence the work reported in this paper.

☐The authors declare the following financial interests/personal relationships which may be considered as potential competing interests: